Eur. Phys. J. C 19, 693–708 (2001)
Digital Object Identifier (DOI) 10.1007/s100520100613

THE EUROPEAN PHYSICAL JOURNAL C

Diffraction at HERA and the confinement problem

J. Bartels[1], H. Kowalski[2]

[1] II. Institut für Theoretische Physik, Universität Hamburg, 22761 Hamburg, Germany
[2] Deutsches Elektronen Synchrotron DESY, 22603 Hamburg, Germany

Received: 7 December 2000 / Published online: 6 April 2001 – © Springer-Verlag 2001

Abstract. We discuss HERA data on the high energy behavior of the total $\gamma^* p$ cross section and on diffraction in deep inelastic scattering. We outline their novelty in comparison with diffraction in high energy hadron-hadron scattering. As a physical picture, we propose an interpretation in terms of QCD radiation at small and large distances: a careful study of the transition between the two extremes represents a new approach to the QCD confinement problem.

1 Introduction

Quantum Chromodynamics (QCD) is expected to describe the strong forces between hadrons. In particular the theory should be able to explain high energy scattering processes. At short distances, smaller than the proton radius, QCD describes the interaction between quarks and gluons in an analogous way to that in which Quantum Electrodynamics provides a quantitative description of the interaction between electrons and photons. High energy processes, however, are often dominated by the forces at large distances (of the order of the proton radius), where a satisfactory understanding of QCD still remains a challenge. One of the main difficulties is the lack of information about the transition from small to large distances. Here results of HERA experiments at DESY in Hamburg are providing unexpected help.

In the past, theoretical efforts to understand the dynamics of confinement have mainly been concentrated on analyzing the binding forces between *static* quarks: the bound states of a quark and an antiquark or of three quarks. The knowledge of these forces, which often are conveniently described in terms of an *interquark-potential*, would allow the calculation of masses and other static properties of hadrons - certainly one of the central problems of strong interaction physics. However, in *high-energy scattering experiments* the question of the binding forces shows up in a somewhat different form. For example, if two protons collide at high energies, usually a large number of tracks of single particles and sometimes of jets are seen in the detectors. This is not surprising if one remembers the well-known picture of sophisticated mechanical Swiss watches: if two such complex objects collide head-on at high energies, one certainly expects to find, after the collision, only the debris of the watches, and one has little hope that the watches remain intact. The higher the energy of the collision process, the smaller the probability of finding the incident projectiles undamaged after the collision. However, in the high energy hadron-hadron scattering processes one also observes a rather large fraction of events in which the incoming particles scatter at very small angles and remain practically intact (called "diffractive"): they either remain completely intact (elastic scattering, about 20%) or they go into an excited state with the same quantum numbers (called "quasielastic", about 10%) Furthermore, these fractions remain almost constant with energy. These observations clearly reflect fundamental properties of the binding forces inside the hadrons which cannot be described by the concept of the interquark-potential.

In the analysis of a high energy scattering process we should distinguish, as in the static confinement problem, between short and long distances. With nucleons as incoming projectiles the scattering process is dominated by distances of the order of the proton radius: all our experience with elastic scatttering at hadron colliders, therefore, reflects features of QCD forces at large distances which we cannot yet calculate. On the other hand, HERA experiments investigate the structure of the proton using short wave electromagnetic radiation, real and virtual photons at very high energies. The virtuality of the photon, Q^2, varies between 0 and O(10000) GeV^2 which means that the photons' sizes can be large or very small. HERA measurements, therefore, have opened the door to a completely new class of reactions which, for the first time, allow the investigation of both the short and long distance region in elastic high energy scattering.

HERA experiments have shown that the scattering of a small photon on the proton is different from what we know from hadron-hadron scattering. First, the total cross section exhibits a considerably stronger rise with energy than observed in hadron-hadron scattering. Secondly, the spread of the scattering system in the transverse direction which can be seen as measure of the forces keeping the scattering projectiles intact is quite different from hadron-hadron scattering. Since HERA allows the size of the photon to vary, it is possible to interpolate between short and

large distances; whereas in the small size region the novel features emerge, in the large size region HERA establishes consistency with the basic features of hadron-hadron scattering.

Comparisons with QCD calculations show that the small size region can be described successfully within the framework of perturbation theory. These calculations of elastic high energy scattering at short distances can be formulated as a *radiation problem*: the incoming photon creates a quark-antiquark pair which radiates gluons and further quark-antiquark pairs. The transition from the scattering of a small size photon on a proton to hadron-hadron scattering can then be viewed as the *transition of QCD radiation from small to large transverse sizes*. Thus at HERA we can not only test our understanding of QCD at short distances but also explore the transition into the confinement region. A careful study of QCD radiation at small and large distances presents a new approach to the QCD confinement problem.

In this article we will review various elastic and quasi-elastic processes observed at HERA and discuss their implications for our understanding of the QCD forces at small and at large distances. In order to illustrate the novelty of HERA results it will be useful to begin with a short review of the main properties of "old" elastic hadron-hadron scattering at high energies: they represent the long-distance (nonperturbative) part of the QCD forces. We then turn to the discussion of HERA results and their interpretation in terms of properties of QCD. At the end we briefly comment on the connection with deep inelastic structure functions.

2 Properties of hadron-hadron scattering

We have already mentioned that in hadron-hadron scattering a substantial fraction of interactions (about 30%) is elastic or quasi-elastic, and both the total and the elastic cross sections remain almost constant with energy. Moreover, certain features of the scattering cross sections have been found to be *universal*, i.e. independent of the species of the incoming hadrons. The theoretical ansatz which, within Regge theory, incorporates these observations carries the name "Pomeron". It was invented by the Russian theoretician V.N. Gribov [1] and afterwards named after another Russian theoretician Y. Pomeranchuk.

For the elastic scattering of two hadrons a and b at high energies and small angles the following economic and convenient parameterization of the scattering amplitude has been found:

$$T_{el}^{ab}(s,t) = is\beta_a(t)(s/s_0)^{\alpha_{\mathbb{P}}(t)-1}\beta_b(t) \tag{1}$$

Here s and t, in units of GeV^2, denote the square of the total energy of the hadron-hadron system and the square of the momentum transfer, respectively. In particular, $t = 0$ implies zero scattering angle. In our discussion, we restrict ourselves to small t-values, say $-0.5 < t < 0$ GeV^2. For simplicity we have approximated the phase factor by i, i.e. we ignore the real part of the scattering amplitude. s_0 is a hadronic scale which is frequently chosen to be of the order of 1 GeV^2. The dependence on the species of the incoming hadron is contained in the form factors, $\beta_{a,b}$, for which it is convenient to use a simple exponential ansatz. The observed energy dependence of the cross section can be described by the ansatz for the exponent $\alpha_{\mathbb{P}}(t)$:

$$\alpha_{\mathbb{P}}(t) = \alpha_{\mathbb{P}}(0) + \alpha'_{\mathbb{P}}t = 1 + \epsilon + \alpha'_{\mathbb{P}}t\,. \tag{2}$$

This function has been found to be independent of the species of the incoming hadrons a and b. The two parameters $\alpha_{\mathbb{P}}(0)$ (or ϵ) and $\alpha'_{\mathbb{P}}$, therefore, appear to be fundamental, and they represent universal features of the strong forces that describe the binding of hadrons (in the jargon the parameters $\alpha_{\mathbb{P}}(0)$ and $\alpha'_{\mathbb{P}}$ are called the "Pomeron intercept" and "Pomeron slope", respectively). In the analysis of high-energy scattering processes, these two parameters have a quite different meaning. The first one, ϵ, determines the energy dependence of the elastic cross section:

$$d\sigma_{el}^{ab}/dt|_{t=0} = \frac{1}{16\pi}[\beta_a(0)\beta_b(0)]^2(s/s_0)^{2\epsilon}. \tag{3}$$

Via the Optical Theorem,

$$\sigma_{tot}^{ab} = \frac{1}{s}ImT_{el}^{ab}(s,0) \tag{4}$$

it also describes the energy dependence of the total cross section:

$$\sigma_{tot}^{ab} = \beta_a(0)\beta_b(0)(s/s_0)^{\epsilon}. \tag{5}$$

Various experiments have found the value $\epsilon \approx 0.08$ [2].

To understand the meaning of the second parameter, $\alpha'_{\mathbb{P}}$, we first note that the ansatz for the scattering amplitude, (1), leads to a geometrical interpretation. To see this we first write the elastic cross section in the following form (valid for small t-values):

$$d\sigma_{el}^{ab}/dt = \frac{1}{16\pi}[\beta_a(0)\beta_b(0)]^2 e^{B(s)t}(s/s_0)^{2\epsilon}, \tag{6}$$

where

$$B(s) = 2\,(B_{0;a} + B_{0;b} + \alpha'_{\mathbb{P}}\ln s/s_0) \tag{7}$$

The energy independent terms $B_{0;a}$ and $B_{0;b}$ originate from the form factors of the hadrons a and b; for proton-proton scattering, experimental data require $B_{0;p} \approx 2-3$ GeV^{-2} (if we identify $B_{0;p} = \langle r_{em}^2\rangle/6$, the often quoted value for the proton radius, $R_p = \sqrt{\langle r_{em}^2\rangle} \approx 4$ GeV^{-1}, leads to $B_{0;p} \approx 2.8$ GeV^{-2}). $B(s)$ increases with the scattering energy s, i.e. the exponential decrease of the elastic cross section steepens with increasing energy (this behavior has been observed experimentally and is called "shrinkage"). By introducing the two-dimensional transverse momentum vector $\mathbf{k}$ (with $\mathbf{k}^2 = -t$), the impact parameter vector $\mathbf{b}$, and by writing the scattering amplitude as a Fourier transform of $f^{ab}(s,\mathbf{b})$, $T_{el}^{ab}(s,t) = 4s\int d^2b e^{i\mathbf{kb}} f^{ab}(s,\mathbf{b})$, we arrive at:

$$\begin{aligned} f^{ab}(s,\mathbf{b}) &= \int \frac{d^2k}{16\pi^2 s} e^{-i\mathbf{kb}} T_{el}^{ab}(s,t) \\ &= i\frac{\beta_a(0)\beta_b(0)}{8\pi}\frac{(s/s_0)^{\epsilon}}{B(s)}e^{-\mathbf{b}^2/2B(s)}. \end{aligned} \tag{8}$$

From this it follows that $R^2_{int} = \langle \mathbf{b}^2 \rangle = 2B(s)$ describes the mean-square transverse extension of the scattering system ("interaction radius") or the size of the interaction region (Fig. 1a). In proton-proton scattering, experiments find $B \approx 8$ GeV^{-2} at small energies, and it grows up to $B \approx 12$ GeV^{-2} at $s \approx 5000$ GeV^2 [3]. This geometrical picture can also be formulated directly for the total cross section. From the Optical Theorem it follows that

$$\sigma^{ab}_{tot}(s) = \frac{1}{s} ImT^{ab}_{el}(s,0) = 4 \int d^2b f^{ab}(s,\mathbf{b}). \qquad (9)$$

The gaussian distribution in (8) suggests a picture in which the scattering system is described as a disc oriented transverse to the direction of flight with a b-dependent opacity: the mean radius of the disc is proportional to $\sqrt{B(s)}$. According to 7, $B(s)$ consists of an energy independent part which is given by the radii of the projectiles a and b, and a term which grows with energy: therefore the transverse size of the scattering system increases at high energies. This growth is determined by the universal parameter $\alpha'_{\mathbb{P}}$: it reflects fundamental properties of the strong forces in QCD. Measurements have found the value $\alpha'_{\mathbb{P}} \approx 0.25$ GeV^{-2} [2]. Following this geometric interpretation the total cross section is proportional to the area and to the opacity of this disc. Because of this optical analogy it is customary to name elastic and quasi-elastic reactions "diffractive processes".

Nowadays most physicists have become so accustomed to the observation that the hadronic total cross section increases with energy, $\epsilon > 0$, that it seems obvious, because of the Optical Theorem, to have a substantial amount of elastic or quasi-elastic reactions in high-energy processes. But one could imagine a different world in which the total cross sections fall: this would imply that the cross sections for elastic scattering and diffraction would go to zero too. The observation that the total cross section slowly increases with energy and that diffractive states do not die out at high energies clearly tells us something about the binding forces which keep quarks together: they act in such a way that hadrons often succeed in surviving the collision and stay intact. The second parameter, $\alpha'_{\mathbb{P}}$, which has the dimension of the square of a length and describes the growth of the transverse extension, $B(s)$, of the scattering system, reflects the strength of the binding forces at high energies. This parameter characterizes the confinement forces in QCD as they manifest themselves in elastic high-energy scattering.

Before the advent of QCD theoreticians have already tried to develop an intuitive understanding of these observations [4–6]. These attempts resulted in a physical picture for the space-time evolution of an elastic high-energy scattering process (via the Optical Theorem it then also leads to an intuitive understanding of the total cross section). Using the language of QCD, this (only qualitative) picture can be summarized in the following way. The two hadrons with equal but opposite momenta which undergo an elastic scattering process at high energies break up into clouds of radiation. Within QCD one can imagine that these clouds consist of soft gluons and quark pairs radiated in cascade-like processes; each gluon carries away a small fraction of the large momentum of the incoming hadron. These "nonperturbative" gluons are not small (in the transverse direction), and they cannot be identified with the partons seen in short distance processes. The formation of this radiation cloud has started long before the hadrons enter the collision process: the higher the momenta of the colliding particles the more time is available for the formation of the radiation clouds. As suggested by field theoretical investigations, the interaction between the hadrons is mediated by the interaction between those parts of the radiation clouds which carry the smallest momentum fractions. To emphasize their importance Richard Feynman introduced the notion of "wee partons". The distribution of these wee partons (both in transverse space and in momentum) plays the central role in the scattering process. This parton-like picture of the scattering process leads naturally to the interpretation that the growth of the transverse size of the interaction region, $B(s)$, with increasing energy is the result of a "diffusion" process (indicated by the shaded area in Fig. 1a). The wee partons (which at large transverse distances are better described as a "pion cloud") diffuse towards the surface of the interaction region with the mean square free path length $\alpha'_{\mathbb{P}}$. The variable $\ln s$ plays here the role of time. From what has been said before one should expect that a complete understanding of these wee partons comes close to a full solution of the complex QCD dynamics: the reassembling of the wee partons after the collision process and the subsequent formation of the outgoing bound state, identical to the incoming hadronic states, can be understood only if we understand the strong binding forces. The fact that the two parameters mentioned before are universal strongly indicates that the wee partons inside the radiation cloud are a fundamental aspect of the strong forces in QCD.

Until now it has not been possible to make this picture of a hadronic high-energy scattering process more precise. At the moment we do not know of any possibility to calculate the two fundamental parameters, $\alpha_{\mathbb{P}}(0)$ and $\alpha'_{\mathbb{P}}$, from "first principles". This is not surprising if we remember that the language of quarks and gluons (in short: perturba-

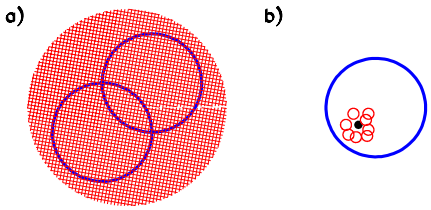

Fig. 1. a Section of the hadron-hadron scattering process in the plane transverse to the direction of flight. The circles denote the hadrons, the shaded area the full interaction region (7): whereas the size of the hadrons stays fixed, the extension of scattering profile grows with energy; **b** Section of the $\gamma^* p$ scattering process in the transverse direction. The big circle denotes the proton, the black dot the virtual photon which creates a $q\bar{q}$ pair and then builds up its radiation cloud which is denoted by the small open circles

tive QCD) can be applied only at small distances and if we recapitulate the geometry of the elastic high-energy scattering process. From the radiation picture that we have introduced it follows that longitudinal and transverse degrees of freedom play quite different roles. Since the formation of the radiation clouds start a long time before the collision (and far away from the interaction region), the longitudinal distances cannot be small. Moreover, the longitudinal extension grows with increasing energy. Theoretical investigations, on the other hand, indicate that it is the size of the transverse distances which determines the magnitude of the strong coupling constant and thus the applicability of perturbative QCD. Incoming hadrons - even before the beginning of any radiation process - have transverse extensions which are large: for distances of the order of a proton radius the strong coupling constant is not small and perturbative QCD does not apply. On top of the "static" hadronic radii, the radiation and formation of wee partons lead to a further (energy dependent) increase in the transverse direction and make the situation even worse. It may help to visualize the elastic hadron-hadron forward-scattering process as taking place inside a long cylindrical tube with its axis along the direction of flight. In hadron-hadron scattering this tube has a large diameter. In a Gedanken-experiment one might imagine having two incoming particles of small transverse sizes: for not too high energies, their scattering would be confined to a tube with a very small diameter (a "femto-tube"), and we could hope to be able to calculate the radiation cloud and the scattering cross section within perturbative QCD.

It was a surprise that HERA measurements can be viewed as a (partial) realization of this Gedanken-experiment. For most readers, HERA is the machine which measures deep inelastic structure functions of the proton. It has turned out that these measurements - when interpreted slightly differently - have opened a new door to the understanding of the strong interactions. In the following section we shall discuss how the short-distance results obtained from HERA measurements differ from the large-distance dominated scattering processes seen in hadron-hadron colliders. Our discussion will be mainly qualitative; a few theoretical remarks will be made in Sect. 3.4.

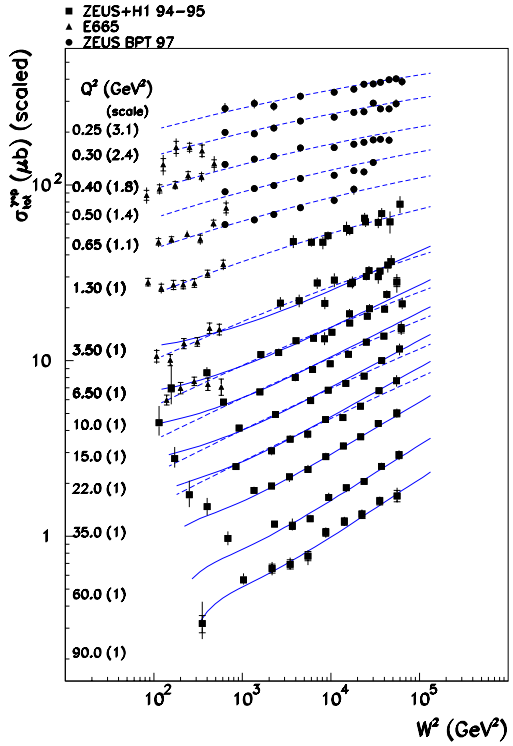

Fig. 2. $\gamma^* p$ cross section as a function of W^2 at various Q^2. The values of Q^2 are shown on the left side together with the scale factor applied to the data for a better visibility. The full line shows a QCD-fit [10], the dashed line shows a fit by a model [13]

3 Properties of the $\gamma^* p$ processes at HERA

Let us first recall that at HERA the electrons collide with protons by emitting highly energetic photons which then hit the proton. Hence, by studying electron-proton collisions, in fact, we investigate photon-proton scattering processes at high energies (in short: $\gamma^* p$) where the photon is highly virtual. The energies of these photons, in the proton rest system, can go up to 50000 GeV. The new feature at HERA is the virtual photon which, compared to pp scattering, has replaced one of the incoming hadrons and which leads to a remarkable advantage. The photons emitted by the electrons can have very small transverse sizes, and HERA offers the possibility to control it. The possible transverse extensions range from a proton size down to about a tenth or a hundredth of it. Such a small photon hits the proton like a sharp "needle"; this is to be compared with a pp-collision, where two "fat" and complex projectiles collide with each other. In this way HERA has brought us closer to the Gedanken-experiment described above: one of the incoming scattering projectiles, the virtual photon, has a small transverse extension. Following our discussion above, we should be able to measure (and compare with our theoretical understanding) the formation of the radiation cloud, the emission of gluons and quark-antiquark pairs, at least in the immediate vicinity of the small photon.

3.1 The total $\gamma^* p$ cross section

One of the most important observations at HERA is the measurement of the total $\gamma^* p$ cross section as a function of the photon virtuality, Q^2, and of the energy of the $\gamma^* p$ system, W (in deep inelastic scattering it is customary to denote this energy by W instead of $\sqrt{s}$). Results are shown in Fig. 2 [7]. The variable $\sqrt{Q^2}$ determines the transverse distance inside the proton that the photon can "resolve", $d \approx \frac{2 \cdot 10^{-14} cm}{Q(GeV)}$. Beginning at the top of our plot with small Q^2-values (large transverse sizes) the photon resembles a hadron, e.g. a ρ-meson. Further below, with increasing Q^2-values, the photon shrinks and becomes more and more point-like. Following the rise of the total cross section in W as a function of Q^2, we observe a striking change. At

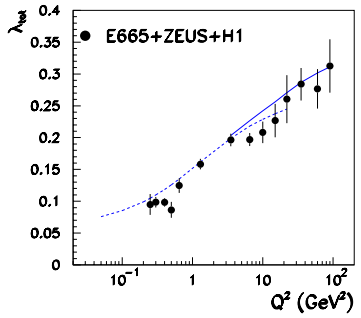

Fig. 3. The exponent λ_{tot} in the parameteriztion $\sigma_{tot}^{\gamma^* p} \sim (W^2)^{\lambda_{tot}}$, plotted as a function of Q^2.The full line shows a QCD-fit [10], the dashed line shows a fit by a model [13]

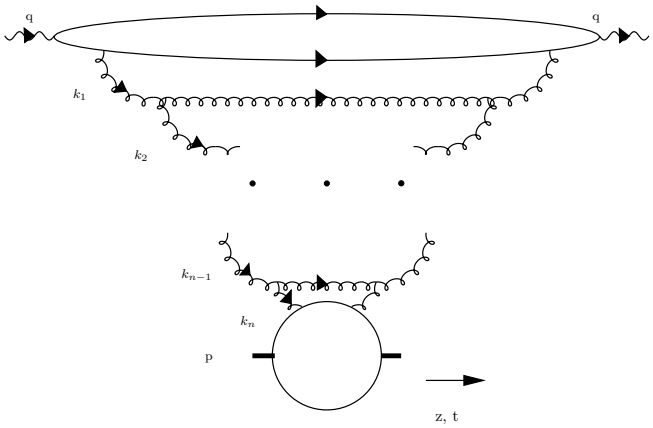

Fig. 4. Space-Time diagram of the elastic $\gamma^* p$ scattering process in the proton rest frame

small Q^2 (our plot begins at $Q^2 = 0.25$ GeV^2) the behavior is still very much the same as in hadron-hadron scattering processes. With increasing Q^2, the rise in W becomes stronger (at the same time the overall magnitude of the cross section decreases). If we parameterize the W-dependence by a power law, $\sigma_{tot}^{\gamma^* p} \sim (W^2)^{\lambda_{tot}}$, this behavior is translated into the Q^2 dependence of the exponent λ_{tot} (Fig. 3). For small Q^2 we find ourselves close to the hadronic value $\lambda_{tot} = \epsilon = 0.08$, whereas for larger values of Q^2 the exponent λ_{tot} increases substantially. In this plot the l.h.s. belongs to the hadronic world, the r.h.s. to the small-distance world where pQCD is expected to apply.

QCD calculations allow the results of the small-distance part (large Q^2 values) to be interpreted in terms of QCD radiation. In particular, the observed growth of the total cross section with energy can be explained in terms of gluon radiation which can be visualized in space and time. We find it advantageous to view the $\gamma^* p$ interactions in the proton rest frame rather than in the more usual infinite momentum frame used in the partonic interpretation of deep inelastic scattering, in which the proton is fast (see Sect. 4). The measured and computed cross sections are, of course, independent of the coordinate system; however, the picture of the process and its intuitive ease of understanding change, depending on the choice of the system. The space-time picture of gluon radiation will be formulated for the elastic γ^*-proton scattering amplitude; the total γ^*-proton cross section follows then via the Optical Theorem.

Viewed in the proton rest system, the incoming photon first fluctuates into a quark-antiquark pair. Subsequently, the quarks start to radiate gluons. The transverse size of the $q\bar{q}$ pair depends on the photon virtuality, Q^2: for our discussion we will be interested in fluctuations of the size $\mathbf{r}^2 \approx 4/Q^2$ (or slightly larger). For $Q^2 > O(10)$ GeV^2, such a $q\bar{q}$ pair is considerably smaller than the proton size of $R_p \approx 4$ GeV^{-1}. For such small distances the strong coupling constant is small, and perturbative QCD can be used reliably. Rather than describing the standard QCD calculations which are done in momentum space, we find it instructive to translate them into space and time variables. The scattering process is illustrated in Fig. 4. The photon moves from the left to the right, and the interaction with the proton takes place at time zero at $z \approx 0$. The lifetime τ of the $q\bar{q}$ fluctuation is given by (see Sect. 3.4):

$$\tau = 1/m_p x. \tag{10}$$

The value of τ becomes large for small x: x is connected with the energy of the $\gamma^* p$ scattering process by $W^2/Q^2 = 1/x - 1$, i.e. small x values mean large energies (in a reference frame where the proton carries a large momentum the variable x denotes the momentum fraction with respect to the proton momentum of the quark struck by the photon). At HERA, for virtual photons with $Q^2 = 10$ GeV^2, the x values range between 10^{-2} and 10^{-4}. The $q\bar{q}$ pair is created at the time $-\tau/2$ before the interaction with the proton, which corresponds to the almost macroscopic distance of up to 1000 Fermi away from the interaction point. Pictorially speaking this means that the $q\bar{q}$ pair exists for a long time and travels a substantial distance while radiating gluons before it finally annihilates back into the final-state photon.

The description of the subsequent radiation processes follows from the analysis of perturbative QCD: the leading QCD diagrams, when translated into time-ordered (old-fashioned) perturbation theory (for more details see Sect. 3.4), lead to a cascade-like time-ordered emission process shown in Fig. 4. Some time after the creation of the $q\bar{q}$ pair, the first gluon with momentum k_1 is emitted, which subsequently emits the second gluon k_2 etc. Whereas the first gluon still has a small transverse size and carries a sizeable fraction of the photon's longitudinal momentum, the later gluons have larger transverse extensions and carry smaller momentum fractions. By the time the $q\bar{q}$ pair reaches the proton, it is surrounded by a system of gluons and has built up its "radiation cloud". The perturbative picture of the cascade processes breaks down when the transverse momentum of the last gluon becomes too small. The precise value, Q_0^2, at which the perturbative development of the cascade stops, is not known. It is customary to assume for Q_0^2 a value of the order of a few GeV^2, i.e. the corresponding transverse distance is smaller than the proton radius. The interaction with the proton at rest is through the last gluon with smallest fraction of the

photon momentum and largest transverse size: its interaction with the proton cannot be described in perturbation theory. Most likely the last gluon further evolves into a nonperturbative cascade of wee partons. After the interaction with the proton it recollects the emitted gluons. The final $q\bar{q}$ pair annihilates into the outgoing photon at time $\tau/2$.

The most striking consequence is that this perturbative gluon radiation explains the observed rise of the total cross section. This rise, therefore, is a measure of the intensity of gluon radiation, and it only weakly depends upon the nonperturbative interaction of the last gluon with the proton. The theoretical analysis of these emission processes results in a simple "QCD radiation formula" (see Sect. 3.4), which leads to a growth of the total cross section with energy. There is a simple way to illustrate this property: assuming, for simplicity, that in the cascade of gluon emissions all transverse momenta are of the same order, and that there is no energy dependence coming from the interaction of the last gluon with the proton, one easily obtains the power law:

$$\sigma_{tot}^{\gamma^* p} \sim \left(W^2\right)^{\lambda}. \tag{11}$$

Although the real calculations are slightly more complicated, the simple power law in (11) describes the data very well, and QCD predicts the right order of magnitude for the exponent λ. Precise QCD descriptions of HERA data are based upon the radiation formula (see (15) in Sect. 3.4), with higher order corrections taken into account. An important example of these corrections is the creation of quark-antiquark pairs inside the radiation cloud: one of the horizontal gluons in Fig. 4 could be replaced by such a quark pair. Moreover, in a precise QCD description of HERA results, data-motivated assumptions are made for the nonperturbative interaction of the last gluon with the proton. The results of such a computation for $Q^2 > 3.5$ GeV^2, shown by the full lines in Fig. 2 and Fig. 3, give a good description of the data. This success of perturbative QCD demonstrates that, for the energy dependence of $\gamma^* p$ scattering, perturbative QCD radiation leads to a much stronger growth of the cross section with energy than the nonperturbative interactions of the last gluon with the proton (inside the circle of Fig. 4).

How could this picture of the gluon radiation around the $q\bar{q}$ pair match with the wee parton picture outlined in the previous section? This is certainly one of the main theoretical challenges raised by the HERA experiments; at present we can only formulate first ideas and conjectures. In order to safely apply perturbative QCD it was essential that the initial photon carried a large virtuality Q^2, and the transverse extension of the produced $q\bar{q}$ pair was small. With each step of gluon emissions, the transverse size of the radiation cloud gets a bit larger, and when it reaches the scale $\sim 1/\sqrt{Q_0^2}$, we enter the nonperturbative region (in Fig. 4 marked by the circle). This suggests that the hadronic-size wee partons which become relevant for the scattering of the last gluon with the proton can be viewed as a continuation of the perturbative gluon cloud into the region of larger transverse distances: the wee partons (which have larger transverse sizes than the perturbative gluons) are certainly present and abundant in this interaction. But their contribution to the rise of the cross section with W, at large Q^2, is considerably weaker than of the perturbative partons. It seems worthwhile to stress that the perturbative QCD radiation cloud supports some of the essential features of the hadronic wee parton picture which, so far, has remained qualitative: the long time scale of the formation of the radiation cloud, and the fact that it is the gluon with the smallest longitudinal momentum fraction which enters the interaction with the proton.

HERA data on $\sigma_{tot}^{\gamma^* p}$ have shown that, when Q^2 changes from large to small values, one observes a fairly smooth transition from the small-size process with the perturbative radiation cloud to the hadron-hadron-like scattering process governed by the nonperturbative wee partons. It therefore seems natural to search, as a function of Q^2, for a continous transition of the perturbative radiation formula to the nonperturbative wee partons. When Q^2 decreases, the following substantial changes are expected. With increasing size of the $q\bar{q}$ pair the perturbative cascade becomes shorter, i.e. it takes fewer steps of emission before the transverse sizes of the radiated gluons reach the boundary of the short-distance region. Furthermore, it becomes likely that the perturbative radiation cloud develops a second cascade. As an example, one of the horizontal gluons in Fig. 4 might start its own cascade, in the same way as the $q\bar{q}$ pair did. In such a scenario the perturbative radiation cloud becomes denser, and a novel state of high-density partons is formed. The creation of this state can then be shown to lead to a weakening of the rise in energy, and this slowdown takes place already inside the short distance part of the radiation cloud, i.e. before long distance effects come into play. This could explain the observed flattening of $\sigma_{tot}^{\gamma^* p}$ with decreasing Q^2. As a consequence, the short-distance part of the radiation cloud looses its dominance over the large size wee partons, and the wee partons begin to play the role known from hadron-hadron scattering. Thus the $\gamma^* p$ process at low Q^2 shows a similar energy dependence as observed in hadron-hadron scattering.

3.2 Diffractive processes at HERA

The analysis of the total cross section $\sigma_{tot}^{\gamma^* p}$ has established that QCD calculations correctly describe the observed energy growth and lead to the picture of QCD radiation at small transverse distances. More has been learned by investigating diffractive final states in $\gamma^* p$ scattering. In the following we will first illustrate that the measurement of the energy dependence of diffractive cross sections fully confirms and extends the interpretation of the total cross section in terms of the radiation cloud. We then turn to the measurement of the transverse interaction sizes which cannot be deduced from the total cross section alone: this is where diffraction at HERA has become most essential.

In the context of deep inelastic electron-proton scattering, diffraction denotes final states where the quark-

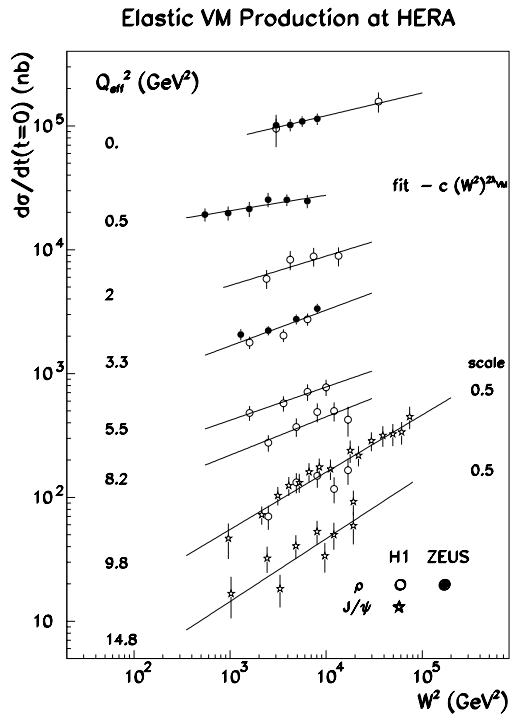

Fig. 5. Cross sections for diffractive ρ and J/Ψ production in the $\gamma^* p$ processes. The data are plotted at a scale Q^2_{eff}, shown on the left hand side of the plot and defined in the text. On the right hand side the scale factor is shown which was applied to the data at $Q^2_{eff} = 9.8$ and 14.8 GeV^2 for better visibility

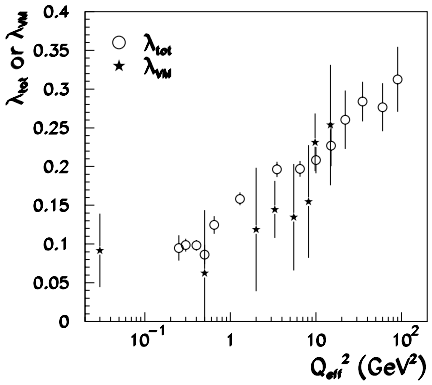

Fig. 6. Comparison of the exponents λ_{VM} and λ_{tot} as a function of the effective Q^2_{eff}; $Q^2_{eff} = Q^2$ for the ρ production and $Q^2_{eff} = Q^2 + M^2_{J/\Psi}$ for the J/Ψ production. The exponents λ_{VM} and λ_{tot} characterize the growth with energy of the diffractive vector meson and total cross section

antiquark pair created by the photon remains well-separated from the proton (the quark pair can also be accompanied by one or more radiated gluons), and turns into a final state which has the same quantum numbers as the initial virtual photon. Examples of diffractive final states at HERA include vector mesons or pairs of jets. As to the proton, in diffraction it either stays intact or turns into an excited state with identical quantum numbers. As a typical feature of the diffractive final state, the invariant mass of the hadronic final state of the photon, M_X, is substantially smaller than the total energy of the γ^*-proton system. In the detector this leads to a visible gap between the diffractive final states of the photon and of the proton ("rapidity gap"). Before HERA it was not expected that diffractive final states in deep inelastic scattering would play a significant role: the energetic virtual photon smashes the proton into pieces, the final state contains large numbers of particles or jets, and it was expected that the $q\bar{q}$-pair created by the photon could hardly be separated from the rest of the final state. In contrast to this expectation, a sizable fraction of diffractive events was observed.

We start our discussion of diffractive processes with vector meson production, $\gamma^* p \to Vp$. At HERA the production of various species of vector mesons has been observed. We will concentrate our discussion on the cross sections for the ρ and J/Ψ production. Similarly to the elastic process, $\gamma^* p \to \gamma^* p$ in Fig. 4, the initial photon first creates a $q\bar{q}$-pair which soon surrounds itself by a radiation cloud. The gluon cloud interacts with the proton in the same way as in the elastic process. However, after the interaction with the proton and the re-collection of the emitted gluons an important difference comes into play: rather than annihilating into a point-like virtual photon (as in Fig. 4), the $q\bar{q}$-pair now creates a vector meson which can have a small or a large transverse size. The size r_V of a vector meson is determined by its quark content, $r_V \sim 1/m_q$ (where m_q denotes the quark mass), and by its wave function. Because of the heavy charm quark, J/Ψ production belongs to the class of small size $q\bar{q}$-pairs (even for the case where the initial photon has a small Q^2 value). The ρ meson, on the other hand, is composed of light quarks, and the size of the $q\bar{q}$ is large; only a point-like photon (with large Q^2, and with a particular polarization) will help to decrease the transverse size of the $q\bar{q}$ pair. HERA results for the energy dependence of vector meson production cross sections are shown in Fig. 5 [8].

For the light vector meson (ρ) we have, for $Q^2 = 0$, a weak energy growth of hadronic cross sections. With increasing Q^2, the energy dependence becomes stronger. For heavy quarks (J/Ψ) the cross section also exhibits the strong increase of a small-size system. In order to make this behavior more quantitative, we parameterize the cross sections as

$$d\sigma^{\gamma^* p}_{VM}/dt \sim (W^2)^{2\lambda_{VM}}. \tag{12}$$

In both cases (light and heavy vector mesons) the exponent λ_{VM} grows with decreasing size of the photon (i.e. with increasing Q^2). Because of the heavy charm quark mass, the production of J/Ψ at $Q^2 = 0$ corresponds to ρ-production at a higher Q^2-scale. A quantitative comparison can be made if we introduce suitable momentum scales. An appropriate choice of scale for the J/Ψ production is $Q^2_{eff} = Q^2 + M^2_{J/\Psi}$, whereas for the ρ production we simply use $Q^2_{eff} = Q^2$. Figure 5 shows that the cross sections for ρ and J/Ψ production are almost the same if we use the scale Q^2_{eff}. Figure 6 shows the values of λ_{VM}

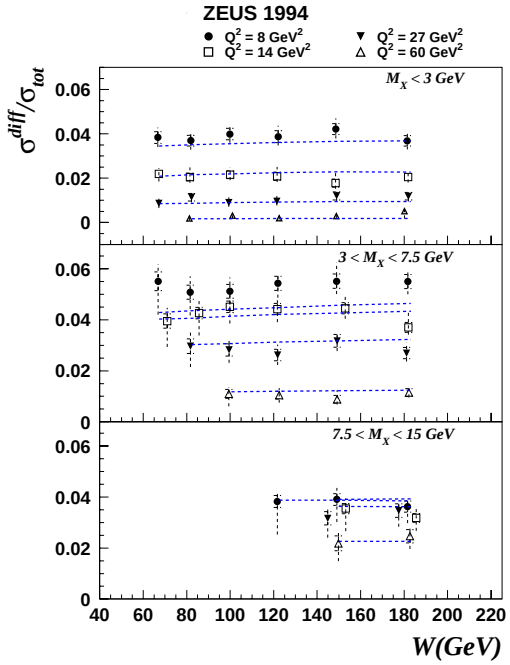

Fig. 7. Ratio of diffractive and total cross sections at fixed values of Q^2, for different regions of the invariant diffractive mass M_X. The lines belong to a model [13] described in the text

determined from data of Fig. 5, at fixed values of Q^2_{eff}, and compares them to the λ_{tot} values of Fig. 3. The figure shows that the rise of the cross sections in different photon-proton processes is strikingly similar in the whole observed Q^2 region. We take this similarity as direct experimental evidence for the universality of the radiation cloud, not only in the high Q^2 region but also in the transition to the low Q^2 region.

Another important observation at HERA is the measurement of the inclusive diffractive cross section, i.e. of the sum of cross sections for all processes which exhibit a rapidity gap. In this measurement the sum extends over very different diffractive final states, vector mesons, open $q\bar{q}$-pairs which turn into jets, $q\bar{q}g$ systems, and others. In order to analyze the space-time evolution of these processes we once more return to our picture of the elastic $\gamma^* p \to \gamma^* p$ process (Fig. 4) and perform suitable substitutions of the final state photon. All these reactions have in common that the initial photon creates a $q\bar{q}$-pair which soon surrounds itself by a radiation cloud. In course of the interaction with the proton at rest, however, an important difference emerges: in the elastic case and in the case of diffractive vector meson production, the transverse size of the $q\bar{q}$ pair was strongly influenced by the outgoing diffractive system (virtual photon or vector meson). For the inclusive cross section, on the other hand, the diffractive final state is free to choose its transverse size, i.e. it can either be small or large. Examples of small-size systems are, once more, the diffractively produced vector particles with heavy quarks. An example of a large-size system is the diffractive production of two jets of light quarks, which are aligned along the $\gamma^* p$ scattering axis. If we follow our discussion above, we expect, for the former case, the cross section to exhibit a strong energy increase, $\sigma_{diff} \sim (W^2)^{2\lambda_{tot}}$. In the latter case, however, we expect the process to be rather hadron-like, with a slowly-rising cross section, $\sigma_{diff} \sim (W^2)^{2\epsilon}$. The inclusive diffractive cross section sums over all these diffractive states with different sizes. Hence, if we define the exponent λ_{diff} by $\sigma_{diff} \sim (W^2)^{2\lambda_{diff}}$, the energy dependence should be somewhere in between the two extremes:

$$\epsilon < \lambda_{diff} < \lambda_{tot}.$$

Correspondingly, the mean transverse extension of the inclusive diffractive final state lies somewhere between small and large sizes. Before HERA it was generally expected that the large-size configurations would give by far the dominant contribution, and λ_{diff} would be very close to the value ϵ. In contrast, measurements at HERA (Fig. 7, [9]) show the striking result that, at fixed Q^2, the ratio of the inclusive diffractive cross section and the total $\gamma^* p$ cross section is nearly constant, i.e. $\lambda_{diff} \approx \lambda_{tot}/2$. Since this value is significantly larger than ϵ, small-size contributions clearly are not negligible. Whereas the above inequality is a rather straightforward consequence of merely qualitative arguments, an explanation of Fig. 7 has come from an interesting theoretical development which will be discussed in Sect. 3.4.

3.3 Transverse sizes

In our discussion of HERA results so far, we have limited ourselves to the forward direction $t = 0$. The mean transverse size $\mathbf{r}$ of the $q\bar{q}$-pair has played the important role of discriminating between "small-size" and "large-size" projectiles. But in our brief summary of hadron-hadron scattering, we discussed another transverse scale, the impact parameter $\mathbf{b}$ with its mean square value being proportional to $B(s)$: it describes the transverse extension (interaction radius) of the scattering system of hadron a and b (Fig. 1a). At HERA the analogue of this parameter is the transverse extension of the scattering system consisting of the quark-antiquark pair and the proton at rest (Fig. 1b). To access this parameter experimentally, we need to measure nonzero scattering angles, i.e. the cross sections at $t \neq 0$. This region cannot be reached for the elastic $\gamma^* p$ scattering process. Because of the Optical Theorem, the measurement of the total cross section provides only the scattering amplitude at $t = 0$. Here diffractive final states exhibit the unique feature of permitting the measurement of the t dependence. In particular, in elastic vector meson production, $\gamma^* p \to V p$, the transverse momentum of the outgoing particles with respect to the $\gamma^* p$ axis can be directly measured.

As we discussed after (7), the slope $B(s)$ of the exponential fall-off of the observed t distribution of the elastic cross section determines the size of the interaction region: $R^2_{int} = 2B(s)$. In Fig. 8 we first show the slope B, at a fixed energy, as a function of the effective Q^2 scale, Q^2_{eff}, for various vector meson production processes [8]. The slope

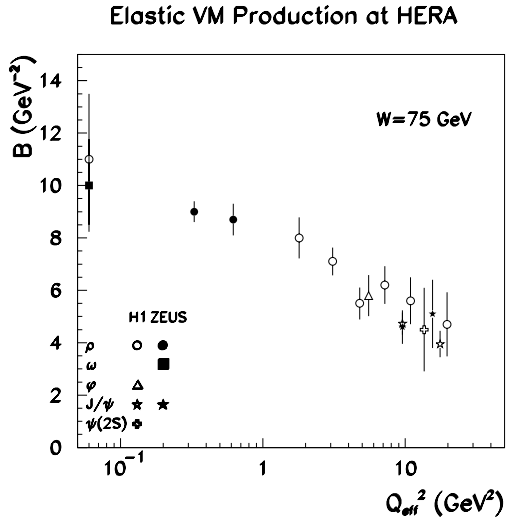

Fig. 8. Slope parameter $B(s)$ as a function of Q^2_{eff}; $Q^2_{eff} = Q^2$ for the ρ and ω meson production, $Q^2_{eff} = Q^2 + M^2_\phi$ and $Q^2_{eff} = Q^2 + M^2_{J/\Psi}$ for the ϕ and J/Ψ production

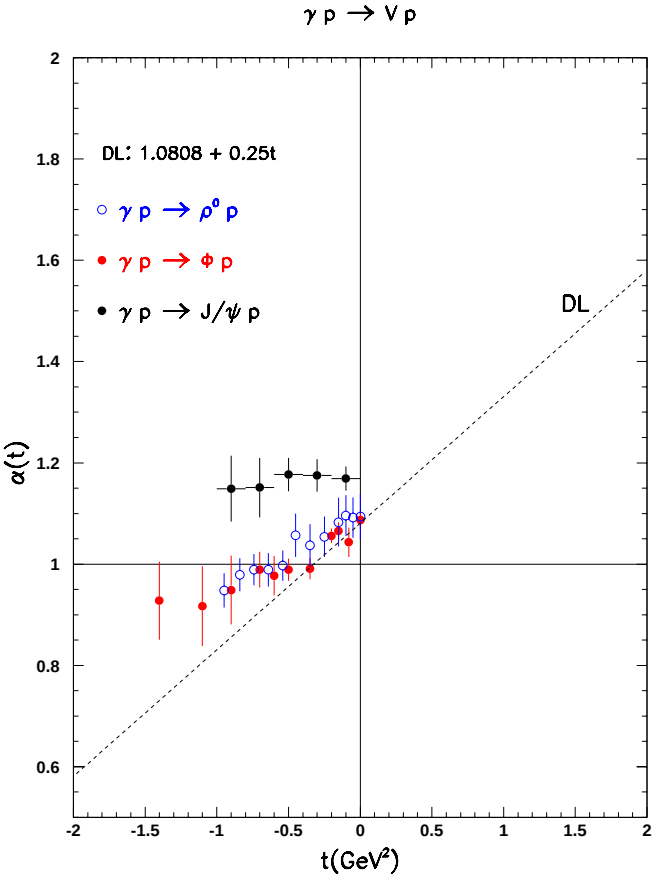

Fig. 9. $\alpha(t)$ for diffractive ρ, ϕ and J/Ψ photoproduction

B (and the size of the interaction region) shrinks with increasing virtuality Q^2_{eff}. In the photoproduction region, $Q^2_{eff} = 0$, the observed B values of ρ and ω are of the order 10 GeV^{-2}, and they are similar to the values observed in proton-proton scattering at high energies (with B of the order $12 - 14$ GeV^{-2}). At higher Q^2_{eff}, the B slopes at HERA become considerably smaller, $B \approx 4 - 5$ GeV^{-2}: this is, approximately, half of the B value observed in proton-proton scattering at low energies, i.e. it corresponds to the "interaction size of a single proton". This suggests that the transverse extension of the scattering system has the form shown in Fig. 1b: the interaction region is determined by the size of the proton, whereas the photon and its quark-antiquark pair (denoted by the black point) have radii much smaller than the proton. Its perturbative radiation cloud (small circles around the black dot) determines the growth of the cross section with energy, and its size is smaller than the proton radius. The nonperturbative continuation of the radiation cloud (not shown), presumably, contains large-size wee partons, but they seem to be "dormant", in that they have little influence on the growth of the total cross section.

Let us next see how the transverse shape of the scattering system evolves with energy. In (2)-(7) we have described, for hadron-hadron scattering, how the t-slope of $\alpha(t)$, the exponent of the energy dependence of the scattering amplitude, leads to an energy dependent contribution to $B(s)$ and thus determines the growth of the scattering system in the transverse direction. Figure 9 shows the measured $\alpha(t)$ dependence as a function of t obtained from a combination [14] of the HERA photoproduction data and from low energy measurements from other experiments. For light vector particles (ρ, ϕ) which have transverse radii of hadronic size the exponent $\alpha(t)$ is rather close to the hadronic Pomeron trajectory $\alpha_{\mathbb{P}}(t)$ (denoted by "DL"). In the case of J/Ψ photoproduction which belongs to the class of small-size diffractive systems the exponent $\alpha(t)$ shows a weaker t dependence, i.e. α' is significantly smaller than $\alpha'_{\mathbb{P}} = 0.25$ GeV^{-2}. We view this smallness of α' for J/Ψ-production as the *second striking difference* in the elastic scattering of small-size and hadron-size projectiles: not only the energy dependence of the scattering cross section at $t = 0$, but also the α' parameter in the exponent exhibits different characteristics. Calculations in perturbative QCD lead to the expectation that α' should be small (Sect. 3.4), i.e. they are in qualitative agreement with the HERA measurement.

In order to obtain a geometric interpretation (in transverse direction) of J/Ψ photoproduction at HERA let us first consider the situation (until now still hypothetical) of a system which has a much smaller size than the J/Ψ system at $Q^2 = 0$. In this case perturbative QCD predicts a vanishing slope parameter α' which, by the arguments given in Sect. 2, leads to the conclusion that the interaction radius does not increases with energy. This is illustrated in the transverse picture shown in Fig. 1b: the proton size does not change with energy, and large-size wee partons whose cloud might grow with energy are "not active". Evolution with energy takes place mainly inside the radiation cloud around the $q\bar{q}$ pair: with increasing energy the number of radiated gluons grows, and the density inside the cloud around the black dot increases.

The key question now is the change of the radiation cloud when Q^2 is taken to be smaller, i.e. the diffractive system becomes larger. Since we do not yet have a satisfactory theoretical understanding, only some first qualitative ideas can be formulated. We start from large Q^2 values illustrated in Fig. 1b, where we have marked only the perturbative part of the radiation cloud around the $q\bar{q}$ pair, which is responsible for the rise of the cross section. The extension of this region is approximately $\sim 1/\sqrt{Q_0^2}$, which is smaller than the proton radius. If we now move to smaller values of Q^2 (larger $q\bar{q}$ pairs), the size of the gluons inside this region will increase, and this will lead to a higher parton density. This favors the changes in the radiation cloud which we have mentioned at the end of Sect. 3.1: additional gluon cascades are generated which damp the increase with energy. As a result, this region is no longer dominant over the large-size wee partons (not shown in Fig. 1b) which were "dormant" at large Q^2 and are now becoming active. For very small Q^2 (and light quark systems), the wee partons have completely taken over, and the scattering system behaves like in hadron hadron scattering.

Returning to the HERA data on the α'-slope in J/Ψ photoproduction, it is tempting to interpret them as the onset of these transition phenomena. The measured α' value is small but, maybe, nonzero: the interaction size could already be slowly growing with energy. Compared to the situation illustrated in Fig. 1b which belongs to the large-Q^2 region, this would mean that the wee partons have started developing their cloud at the surface of the proton. Presently measurements of the α'-slopes in various vector meson processes are in progress, and considerable improvement in data precision is expected.

3.4 Theoretical analysis of the $\gamma^* p$ processes

In this section we discuss in somewhat more detail how, in the proton rest frame, perturbative QCD calculations (which are now well-established) lead to the radiation picture which we have described so far. In the second part we will turn to current (and, naturally, less well-established) ideas on the transition from the small-distance to the large-distance region which are now being studied.

Let us first return to the gluon-emissions illustrated in Fig. 4. As outlined before, the creation of the $q\bar{q}$ pair takes place a long time before the photon reaches the proton target. In order to estimate the lifetime of a $\gamma^* \to q\bar{q} \to \gamma^*$ fluctuation we start from the four momenta of the proton and the photon in the proton rest frame:

$$p^\mu = (m_p, 0, 0, 0)$$

and

$$q^\mu = \left(Q^2/2xm_p, 0, 0, \sqrt{Q^2 + (Q^2/2xm_p)^2} \right).$$

The incoming photon splits into the $q\bar{q}$ pair with momenta approximately equal to zq^μ and $(1-z)q^\mu$ (where $0 < z < 1$), and the energy difference between the photon and the $q\bar{q}$-state (which, according to the rules of old-fashioned noncovariant perturbation theory [15], consists of on-shell quarks) is $\approx xm_p$. Hence we estimate the lifetime as

$$\tau = 1/m_p x \tag{13}$$

which in the low-x part of the HERA region can be very large. In the same way one can show that the time interval between emission and absorption of the gluon with momentum k_1 is shorter than τ, but longer than the corresponding time interval for the second gluon with momentum k_2. This explains the "nested" time structure of gluon emissions shown in Fig. 4.

The further development of the gluon emission processes can be deduced from the QCD Feynman diagrams that give the leading contribution in the high-energy limit of $\gamma^* p$ scattering; in a physical gauge (axial gauge), they have the ladder-like structure shown in Fig. 4, and non-ladder-like diagrams are suppressed. In order to obtain the space time picture, we have to translate the covariant Feynman amplitudes into old-fashioned time-ordered perturbation theory [15]: we write all possible time orderings and find that, in the limit $x \to 0$ ($W^2 \to \infty$), the time ordering shown in Fig. 4 dominates. In these diagrams the momenta are conserved whereas the energies are not (this feature allows, for example, to estimate the lifetime (13) of photon fluctuation). The main result of this "old-fashioned perturbation theory" is the time-ordering indicated in Fig. 4: the emission of the gluon with momentum k_1 happens after the creation of the $q\bar{q}$ pair, the emission of the second gluon (with momentum k_2) is later than the first gluon etc. Taking further into account that quarks and gluons are traveling with the speed of light, one obtains an analogous ordering in the longitudinal spatial direction (z-direction). As a result, the picture in Fig. 4 describes the evolution both in time and in the longitudinal z-direction.

We now return to 4-dimensional momentum space and describe the kinematic region of the emitted gluons. The $q\bar{q}$ pair emits first a gluon with four-momentum k_1. This gluon carries the fraction z_1 (with $0 < z_1 < 1$) of the photon longitudinal momentum q_l, and the transverse component of its momentum, k_{1t}, is on the average somewhat smaller that $\sqrt{Q^2}$. In the next step this first gluon emits a second gluon with momentum k_2, which carries a fraction z_2 of the photon longitudinal momentum (with $0 < z_2 < z_1$) and has a transverse momentum, k_{2t}, which is on average somewhat smaller than k_{1t}. The probability to emit a gluon in the ith step of this cascade is found to be proportional to

$$\frac{3\alpha_s}{\pi} \int dy_i \int \frac{d^2 k_{it}}{k_{it}^2} \tag{14}$$

where α_s denotes the strong coupling constant and y_i the rapidity of the emitted gluon, $y_i \approx \ln(z_i W^2/k_{it}^2)$. In each step of this cascade the longitudinal and transverse momenta of the gluons decrease. The perturbative cascade process breaks down when the transverse momentum of

the last gluon becomes too small. It is customary to assume for Q_0^2 a value of the order of a few GeV^2, such that the transverse size of the last gluon with momentum $k_{nt}^2 \approx Q_0^2$ is still substantially smaller than the proton. This last gluon, which interacts with the proton in a non-perturbative way, carries the smallest fraction of the large photon momentum and, among the partons of the perturbative cascade, comes closest to the wee parton described in Sect. 2. After this last gluon has finished its interaction with the proton all the emitted gluons are reabsorbed into the $q\bar{q}$ pair which at the time $\tau/2$ annihilates again into the virtual photon. With increasing energy the cascade of gluon emission becomes longer: more and more gluons are emitted.

Before we write down the full expression for the emission of the $n-1$ gluons shown in Fig. 4 we note that, from general rules of quantum field theory, the radiation of a single field quantum of spin J produces a total cross section proportional to $\left(W^2\right)^{2J-2}$. Since the gluon carries spin 1, the radiation of the first gluon already produces a constant total cross section, and each additional radiation will lead to a further logarithmic enhancement. The sum over n of the Feynman diagrams shown in Fig. 4 leads, in the limit of high Q^2 and low x, to the following simplified "radiation formula":

$$\sigma_{tot}^{\gamma^* p} = C \sum_n \left(\frac{3\alpha_s}{\pi}\right)^n \int dy_1 \int \frac{dk_{1\,t}^2}{k_{1\,t}^2} \ldots \int dy_{n-1} \int \frac{dk_{n-1\,t}^2}{k_{n-1\,t}^2} \int dy_n \varphi(y_n, Q_0^2). \quad (15)$$

C denotes the n-independent normalization factor which is of no importance for our present discussion. The factor $\varphi(y_n, Q_0^2)$ describes the y_n dependence of the interaction of the last gluon with the proton, resulting from the wee partons inside the proton which we cannot calculate. The emission of gluons is ordered in rapidities since the y_i values are determined by the fractions z_i of the photon longitudinal momenta carried away by the gluons, and the z_i are ordered. This defines the integration limits in y:

$$0 < y_n < \ldots < y_1 < \ln(1/x). \quad (16)$$

The upper limit is given by the largest possible value of rapidity, $\ln(W^2/Q^2) \approx \ln(1/x)$. In order to illustrate the most important feature of the radiation formula, the rise at small x, we first present a very simplified argument. We will assume $\varphi(y_n, Q_0^2) \equiv 1$, neglect the decrease of the transverse momenta, and we make the assumption that the integrals over the transverse momenta are independent of each other and range from the low momentum scale Q_0^2 up to Q^2. One easily sees that the radiation formula (at fixed Q^2) then leads to the simple power behavior

$$\sigma_{tot}^{\gamma^* p} \sim (1/x)^\lambda \quad (17)$$

with $\lambda = b\frac{3\alpha_s}{\pi}$, $b = \int_{Q_0^2}^{Q^2} \frac{dk_t^2}{k_t^2}$ (the ordering of rapidities gives the factor $1/(n-1)!$ which allows to exponentiate in 15). The value of λ, because of the k_t integration limits, is expected to increase with Q^2. The relation (17) is equivalent to the relation $\sigma_{tot}^{\gamma^* p} \sim \left(W^2\right)^\lambda$ since in the low x region $1/x = W^2/Q^2$.

In order to be more accurate we have to go one step further and discuss, in the radiation formula (15), the range of integration of the transverse momenta which depends upon details of the kinematic limit. So far we have not been very explicit about this aspect: in order to have a small-size incoming photon we have to consider large Q^2 values. On the other hand, we want to have large energies W; this leads us to the combined limit of large Q^2 and small x. Depending now upon the precise order of these two limits, two different restrictions on the transverse momentum integration are obtained. In the classical deep inelastic limit ("Bjorken limit") one first takes Q^2 large, then x small. In this limit one finds the following ordering of the transverse momenta:

$$k_{nt}^2 < k_{n-1t}^2 < \ldots < k_{1t}^2 < Q^2. \quad (18)$$

Alternatively, one considers first x to be small, then Q^2 to be large. In this case the transverse momenta are not ordered. For simplicity we choose:

$$Q_0^2 < k_{it}^2 < Q^2, \; i = 1, \ldots, n \quad (19)$$

(in this case we also have to modify the emission formula (15) by a kernel $K(k_i, k_{i+1})$). If these restrictions are taken into account we find for the radiation formula:

$$\sigma_{tot}^{\gamma^* p} \sim \left\{ \begin{array}{ll} \exp\sqrt{\frac{4\alpha_s N_c}{\pi} \ln 1/x \ln Q^2/Q_0^2} & (DGLAP) \\ (1/x)^\lambda & (BFKL) \end{array} \right\}, \quad (20)$$

where the former case (called DGLAP [16]) belongs to the Bjorken limit, the latter one (called BFKL [17]) to the other ordering of the two limits. Both prescriptions lead to a strong growth of the cross section in $1/x$. At large Q^2 values, the DGLAP case applies. But at lower Q^2 and very small x values the HERA kinematic region, most likely, lies on the interface of the two limits. In both cases, the simple formula (15) leads to a growth of the total $\gamma^* p$ cross section and explains the observed rise.

A closer look at the transverse momenta also allows the spatial extension in the transverse direction to be understood. Transverse momenta are conjugate to transverse distances: the fact that the transverse momenta of the emitted gluons start by being large, then decrease from one emission to the next, implies that the mean transverse distance between two subsequent steps of emission grows. Therefore the radiation cloud of the incoming photon, which started off as a small $q\bar{q}$ pair, grows in the transverse direction. Since the mean separation between steps of gluon emissions grows, this growth is faster than, e.g., in normal diffusion. When the transverse momenta of the emitted gluons become small, perturbative QCD ceases to be applicable: the scale Q_0^2 at which this happens corresponds to a spatial transverse extension which has to be smaller than the proton radius. For larger transverse distances, most likely, the evolution of the radiation cloud continues: in (15) this long-distance part of the radiation cloud is parameterized by the function $\varphi(y_n, Q_0^2)$,

and it has its own (weak) energy dependence which has to be taken from experimental data. This discussion leads us to the picture illustrated in Fig. 1b: the incoming photon (denoted by the black dot) is much smaller than the proton. It is surrounded by its perturbative radiation cloud (denoted by small circles) which produces the strong increase of the cross section with energy. Its long range, nonperturbative part (not shown) reaches the full proton size: its influence on the energy dependence of the total cross section is much weaker than that of the perturbative part of the cloud.

To finish our summary of perturbative QCD calculations we have to address the question of the t-dependence of the scattering amplitude. The main result is that, for small-size photons and small momentum transfer, the energy growth of the scattering amplitude varies only little with t. This can easily be made plausible by generalizing the QCD radiation formula to nonzero momentum transfer. Let us consider a small momentum transfer (e.g. $|t| < 0.5$ GeV^2). Starting from Fig. 4 we give the incoming and outgoing photons small transverse momenta, $-\mathbf{k}/2$ and $\mathbf{k}/2$, resp., with $t = -\mathbf{k}^2$. Correspondingly, the gluons on the l.h.s. (with four momenta $k_1, ...k_n$) carry the additional transverse momentum $-\mathbf{k}/2$. We have argued, in order to obtain the radiation formula, the transverse momenta have to be large (up to the order of $\sqrt{Q^2}$): this means that, to a good approximation, the small momentum transfer $\mathbf{k}/2$ can be neglected, and the result for the energy dependence remains practically unchanged when going from $t = 0$ to $t \neq 0$. The same argument can (approximately) be used for diffractive J/Ψ-production, and it explains the observed small t-slope α' of the trajectory $\alpha(t)$ shown in Fig. 9. Following our previous argument for the geometric interpretation of $\alpha(t)$, we therefore conclude that the transverse extension of the scattering system shown in Fig. 1b does not increase with energy: the density of the gluons around the $q\bar{q}$ pair increases, but the transverse radii of the pertubative cloud and of the proton remain constant.

This completes our discussion of the small-size scattering process (photon with large Q^2 or vector meson with heavy quarks). We now turn to the transition to large distances. This is where theoretical interest is now focused, and for which intensive comparisons with experimental data are being made. We have already indicated what kind of ideas are being pursued: at low Q^2, before the perturbative radiation cloud (consisting of a single gluon cascade) develops into the nonperturbative cloud of wee partons, we first expect to see the beginning of 2, 3,... cascades which lead to the production of a large number of gluons. In other words, we expect that before the long-distance physics of QCD confinement begins we may see an intermediate region which can be addressed still using quark and gluonic degrees of freedom. One of the main characteristic features is the high density of gluons which generates a strong gluon field. If true, this is a rather remarkable state: on the one hand, it is still dominated by rather short distances where typical confinement effects (e.g. chiral symmetry breaking and the formation of pion pairs which are an essential part of the nonperturbative wee partons) can be disregarded. On the other hand, the high density of gluons creates a strong field and leads to sizable cross sections. This expectation is based upon extensive studies of higher order QCD corrections to the single-cascade picture shown in Fig. 4 [18]. In order to give an intuitive motivation for the appearance of this novel high-density state in QCD, let us consider a situation where, at fixed large Q^2, x becomes extremely small, much smaller than at HERA. Since the increase of the total $\gamma^* p$ cross section with energy, as predicted by the single gluon cascade, cannot continue forever, there must be some corrections which slow down the rise. The one-cascade picture can be valid only if the system of gluons is sufficiently dilute. When at very small x the gluon density of the single cascade becomes too high, interactions with other cascades (which are always present but, in the standard case of not so small x, are simply not noticed by the proton) will become important. An example is the formation of two separate gluon cascades: after the emission of the first gluon (in Fig. 4 with momentum k_1) which initiates the first cascade of gluon emissions, the $q\bar{q}$-pair radiates a second gluon which begins its own cascade. This formation of two branches of gluon radiation becomes relevant when the offsprings of both cascades have a chance to simultaneously find partners inside the proton. Such pairwise (coherent) interactions of both clouds lead to negative interference effects and damp the energy growth of the cross section. As x decreases further, more and more cascades are formed; the rise in $1/x$ of the gluon density becomes weaker, and the gluon density could even become flat in $1/x$, i.e. it reaches "saturation". This interplay of a large number of cascades which leads to saturation effects has to be viewed as a precursor of confinement: once saturation has eliminated the dominance of the small-size part of the radiation cloud, the large size (of the order of the proton radius) wee partons and long-range properties of the QCD vacuum become important, and quarks and gluons are no longer the suitable degrees of freedom to describe the radiation cloud.

It is very plausible to expect that the energy value at which these saturation effects set in will go up as Q^2 increases: the smaller the transverse size of the $q\bar{q}$ pair and of the radiated gluons, the longer the cascade will grow before the state of high density is reached and the formation of additional gluon cascades becomes relevant. Conversely, at low Q^2 saturation sets in earlier: this suggests that the observed damping of the growth of the cross section at low Q^2 (or at least its beginning) may be due to this same saturation mechanism [11]. The success of a simple model, described below, supports this conjecture.

As we have said before, these questions are currently under investigation. Most recently, attempts have been made to find a phenomenological *interpolation formula* which, by comparing to HERA data, could test these ideas. For such an attempt it is useful to have a formalism which is general enough to provide a bridge from small to large transverse distances and to apply to both the total cross section and to the diffractive cross sections. In the proton

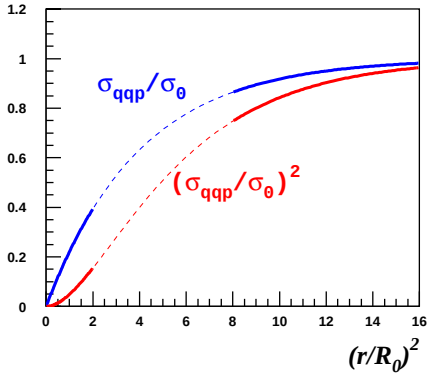

Fig. 10. The dipole cross section $\sigma_{q\bar{q}p}$ of [13] as a function of the transverse extension of the quark-antiquark pair. The lower graph shows the square of this cross section which is relevant for the inclusive diffractive process

rest frame the total cross section, to good approximation, can be written in the following form:

$$\sigma_{t,l}^{\gamma^* p}(x,Q^2) = \int d^2\mathbf{r} \int dz\, \psi(Q^2,z,\mathbf{r})^*_{t,l} \times \sigma_{q\bar{q}p}(x,\mathbf{r}) \psi(Q^2,z,\mathbf{r})_{t,l}, \qquad (21)$$

where $\psi(Q^2,z,\mathbf{r})_{t,l}$ denotes the transversely (t) and longitudinally (l) polarized photon wave-function, $\sigma_{q\bar{q}p}(x,\mathbf{r})$ the dipole cross section of the interaction of the $q\bar{q}$ pair with the proton, z the momentum fraction of the photon carried by the quark, $0<z<1$, and $\mathbf{r}$ the transverse size of the quark-antiquark pair. The wave functions are solely determined by the coupling of the photon to the quark pair, and they are well known in QED. Equation (21) corresponds to the physical picture that we have drawn: the incoming virtual photon creates a quark-antiquark pair (expressed in terms of the photon wave function ψ), the $q\bar{q}$ pair interacts with the proton (denoted by $\sigma_{q\bar{q}p}$), and finally annihilates into the outgoing virtual photon (ψ^*). All interesting dynamics (gluon radiation etc.) is encoded in the $\mathbf{r}$ and x dependence of $\sigma_{q\bar{q}p}$. For small $\mathbf{r}$ we have the gluon radiation which we can calculate in perturbation theory, and we find that the cross section is approximately proportional to $\mathbf{r}^2$. At medium $\mathbf{r}$ values we expect to see the beginning of "saturation" that we have sketched before, and for large $\mathbf{r}$ the dipole cross section has to become rather flat in order to agree with the observed weak energy growth of the hadronic cross section at low Q^2. In (21) the main contribution of the $\mathbf{r}$ integral comes from distances $|\mathbf{r}|$ around (or slightly larger than) $2/\sqrt{Q^2}$.

The dipole cross section $\sigma_{q\bar{q}p}$ can also be used to describe diffractive processes, in particular vector meson production or the inclusive diffractive cross section (in the forward direction $t=0$). For example, the integrated cross section of diffractive $q\bar{q}$ production can be expressed in terms of the dipole cross section:

$$\frac{d\sigma_{Diff}^{\gamma^* p}}{dt}\Big|_{t=0} = \frac{1}{16\pi} \int d^2\mathbf{r} \int dz\, \psi(Q^2,z,\mathbf{r})^* \times \sigma_{q\bar{q}p}^2(x,r^2)\, \psi(Q^2,z,\mathbf{r}) \qquad (22)$$

This expression does not depend any more on any wave-function of the diffractive final state: the $q\bar{q}$ pair is no longer forced into a final state of a given size (as it was, for example, the case for vector particles), but can choose rather freely its preferred size. A large fraction of the events, in fact, selects configurations in which the quarks have rather large transverse extensions ("aligned jets"). In contrast to the total cross section formula, (21), which is linear in the dipole cross section, the inclusive diffractive cross section, (22), contains the square. As we have mentioned before, in any dipole model at small $\mathbf{r}$ the cross section is approximately proportional to $\mathbf{r}^2$. Therefore the contribution of final states with small $\mathbf{r}$ is suppressed in comparison with the total cross section (for an example see Fig. 10: $(\sigma_{q\bar{q}p}/\sigma_0)^2 \ll \sigma_{q\bar{q}p}/\sigma_0$ at $r \ll 2R_0$). This is in agreement with the observed large transverse size of the inclusive diffractive process ($B \approx 7$ GeV^{-2} at $Q^2 > 5$ GeV^2 [12]).

We conclude our discussion with a recent model [13] for the dipole cross section which has been built on the idea of saturation and which has turned out to provide a very successful description of the HERA data in the low Q^2 region. The ansatz for the dipole cross section is:

$$\sigma_{q\bar{q}p}(x,\mathbf{r}) = \sigma_0 \left(1 - \exp\left[-\frac{r^2}{4R_0^2}\right]\right), \qquad (23)$$

where R_0 denotes the (x-dependent) dipole size where saturation sets in ("saturation radius": $R_0^2 = R_0^2(x) = \frac{1}{Q_0^2}\left(\frac{x}{x_0}\right)^{\lambda_{GBW}}$ with $Q_0 = 1$ GeV). Figure 10 shows the graphic representation of $\sigma_{q\bar{q}p}$. The parameters of the model, σ_0, x_0, and λ_{GBW}, were determined from the fit to the total cross section data: $\sigma_0 = 23mb$, $\lambda_{GBW} = 0.29$, and $x_0 = 3 \cdot 10^{-4}$. The dashed curves in Fig. 2 and Fig. 3 show that in the low-Q^2 region the energy dependence of the total cross section is very well described by the model. The model has also been used for diffraction: when the formula for the dipole cross section is inserted into (22), it leads to a good description of the diffractive cross section for $q\bar{q}$ production. In particular, as a result of a subtle interplay between the photon wave function and the dipole cross section, it succeeds in reproducing the energy dependence shown in Fig. 7 (note that the results of the model shown in this figure are genuine predictions, since all the parameters of the model have already been fixed by the measurements of the total $\gamma^* p$ cross section).

Although the dipole formula in 23 should primarily be considered as a phenomenological parameterization of the transition region between small and large sizes of the $q\bar{q}$-pair, it nevertheless illustrates some features of the peculiar "high density" region. First, for small dipole sizes r one sees the dipole behavior $\sim r^2$. Next, if we increase the energy (i.e. we go to very small x, beyond the HERA region), R_0 becomes rather small, and the exponent in the dipole formula is of order unity even for small dipole sizes $\mathbf{r}^2 \approx 4R_0^2$: since $\sigma_0 = 23$mb is a large cross section (comparable to the πp total cross section), we arrive at a large dipole cross section already in the region of small distances, $\mathbf{r}^2 \approx 4R_0^2 \ll R_p^2$, where typical long distance

confinement effects are not yet expected to be important. This large cross section is rather due to the high gluon density which produces a strong gluon field. A more detailed analysis, in fact, allows the dipole cross section formula, (23), in this intermediate region to be interpreted as a sum of multi-gluon cascade contributions, very much in the way we have outlined before. For dipole sizes larger than R_0, we can disregard the exponential term: this is then the long-distance region where confinement holds. The success of this simple model indicates that the gross features of the physical picture which underlies this dipole model must be correct. The next step could be a generalization to nonzero momentum transfer: this addresses the generation of the slope parameter α'. We have argued before (and seen in the data) that in the perturbative region α' is small. But we also know that at large distances it has to approach the hadronic value $\alpha'_{\mathbb{P}} = 0.25$ GeV^{-2}. Understanding the origin of this confinement parameter presents the most challenging task.

Summarizing this "theoretical section", we have shown that QCD calculations are in qualitative (partially also quantitative) agreement with the small distance parts of the observed $\gamma^* p$ scattering. HERA data at low Q^2, which probe large distances, are fully consistent with previously observed hadron-hadron scattering. We therefore have to develop a formulation which allows an interpolation between the perturbative QCD calculations at short distances and the nonperturbative features of hadron-hadron scattering at large transverse distances. The suitable physical picture is *radiation*: at small distances QCD calculations, when interpreted in the proton rest frame, lead to the simple picture of a *radiation cloud of the incoming photon*, and at large distances we know the general features of the wee partons which again fit into the framework of radiation. For the transition from the perturbative QCD region to the confinement region we have precise data which allow a test of any theoretical hypothesis. On the theoretical side there is the well motivated expectation that between the regions of perturbative QCD and confinement dynamics there exists a novel region of "high density partons". The simple saturation model [13] which is based upon these ideas has turned out to be very successful and thus provides phenomenological support for the underlying dynamical mechanism.

4 Deep inelastic structure functions

How is this picture of a "radiation cloud of the incoming photon" related to the concept of the "deep inelastic proton structure function"? The precise measurement of these structure functions and of parton densities in a wide kinematic region is one of the important goals at HERA. Parton densities present probability densities for finding partons (quarks or gluons) with specified momentum fractions and transverse extensions inside the proton. In order to have an intuitive picture of "partons inside the proton" we have to go into another Lorentz-frame, the so called Bjorken frame, in which the proton has a much larger

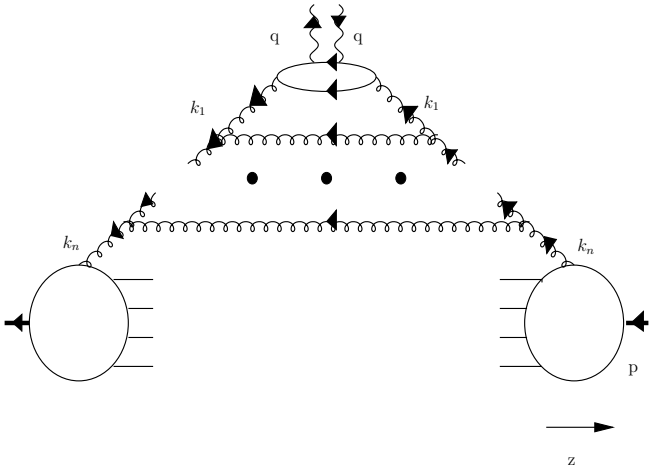

Fig. 11. Space-Time diagram of the elastic $\gamma^* p$ scattering process in the deep inelastic (Bjorken) frame

longitudinal momentum than the photon. In this frame the four momenta have the form:

$$p^\mu = \left(\sqrt{p^2 + m_p^2}, 0, 0 - p\right), \tag{24}$$

(with a very large p) and

$$q^\mu = \left(Q^2/2xp, \mathbf{q_t}, 0\right), \tag{25}$$

with $\mathbf{q}_t^2 \approx Q^2$. The space-time picture of the process is obtained in the same way as in in the proton rest frame: the dominant QCD Feynman diagrams are translated into time-ordered (old-fashioned) perturbation theory for which it can be shown [15] that only the time-ordered diagrams of Fig. 11 contribute to the high energy limit. Therefore now it is the proton (moving in the negative z-direction) which, long before it interacts with the photon, starts to build up its radiation cloud. Since the transverse extension of the proton is large, the birth of this cloud cannot be described in terms of perturbative quarks and gluons. Only at a later stage of the formation process, when perturbative partons with sufficiently small transverse extensions have been created, can this language start to be used. This "final" perturbative part of the radiation process is illustrated in Fig. 11. Among these partons the incoming photon has to find its partner with longitudinal momentum equal to the fraction x of the proton momentum, and with the large transverse momentum, $Q_0^2 \ll k_t^2 \ll Q^2$, The lifetime of the $q\bar{q}$ fluctuation which interacts with the photon can be estimated as $\tau_{q\bar{q}} \approx xp/\langle k_t^2 \rangle$. It is considerably longer than the time between the absorption and emission of the virtual photon, $\tau_\gamma = 1/q_0 \approx 2xp/Q^2$: the parton cloud remains "frozen" during the interaction and can be precisely scanned by the virtual photon.

The structure functions and parton densities obtained from the HERA data extend into kinematic regions which had not been measured before, in particular the region of very small x (i.e. large energy of the $\gamma^* p$-subprocess) and low Q^2. The results which we have discussed in Sect. 3 can

easily be translated into the deep inelastic picture. Using the relation

$$\sigma_{tot}^{\gamma^* p} = \frac{4\pi^2 \alpha_{em}}{Q^2} F_2(x, Q^2), \tag{26}$$

the observed strong growth with the energy of the total $\gamma^* p$ cross section is re-phrased as an increase of the deep inelastic structure function F_2 at small x. One of the important questions which still need to be answered is the limit of the applicability of the concept of parton densities: for small Q^2 (where the photon becomes hadron-like) the notion of partons and QCD perturbation theory breaks down, and we still have to determine more precisely how far down in Q^2 and x the standard QCD analysis of deep inelastic scattering works.

A comparison of this "deep inelastic" interpretation in the Bjorken frame with our previous discussion based upon the proton rest frame illustrates a very interesting feature. In the "deep inelastic picture" the radiation cloud results from the break up of the incoming proton and can therefore be named the "radiation cloud of the proton". In contrast, in the proton rest frame we have been discussing the "radiation cloud of the photon". When comparing the two pictures, one finds that it is mainly the time variable which plays different roles. On the other hand, we know that the two pictures are completely equivalent: they are both derived from the same QCD calculations at small x (or large energies W), by first choosing a frame and then translating the Feynman diagrams into space time variables. The cross section formulae are, obviously, frame-independent. The equivalence of the two pictures implies that the radiation cloud belongs to both the proton and the photon simultaneously. This supports Feynman's conjecture that in a hadron-hadron collision the nonperturbative wee partons belong to both projectiles and are a fundamental part of the underlying strong forces.

For our discussion we found it more suitable to use the proton rest frame with the "radiation cloud of the photon". In order to follow the transition from radiation at short transverse distances to large transverse distances we found it instructive to chose that picture where the beginning of the radiation cloud can be analyzed within perturbative QCD. Later on, when the evolution of the radiation cloud enters the nonperturbative region, we have some knowledge based upon the wee parton analysis of high-energy hadron-hadron scattering.

5 Summary and outlook

Measurements at HERA have opened a new route to understand the confinement problem by the investigation of processes in which virtual photons with variable transverse sizes interact with protons at high energies. For photons with small transverse sizes, the measured cross sections exhibit a considerably faster growth with energy than in hadron-hadron scattering; this feature can be explained within perturbative QCD. HERA data on diffraction show another important property: a scattering system consisting of a small-size vector particle and the proton has a transverse extension which is not larger than a single proton, and, in contrast to hadron-hadron scattering, it does not expand as energy increases. This observation is also in agreement with perturbative QCD expectations. The picture appropriate to understand these scattering processes is that of radiation: in the proton rest frame the perturbative QCD calculations can be formulated in terms of a radiation cloud of gluons and quarks which are emitted within a femto-tube around the incoming virtual photon. For the first time in high-energy physics experiments, it is possible to understand the high energy behavior of cross sections which are mediated by the strong forces.

The transverse size of the incoming photon can be varied continuously. For photons with large transverse extensions, the cross sections show the same characteristics as observed in hadronic processes. The energy dependence of the cross sections in hadronic processes has long been known to have universal properties (attributed to the "Pomeron"). Attempts to understand the dynamics of this branch of strong interaction physics led, long before HERA, to an intuitive space-time picture of hadron-hadron scattering in which the radiation of wee partons plays an essential role. This picture is strongly supported by the perturbative QCD cloud at short distances. A central task posed by HERA measurements is the need to understand the transition between QCD radiation at short distances and the nonperturbative wee parton dynamics at large transverse distances. The HERA measurements and their theoretical interpretation show that high-energy scattering can be viewed as QCD radiation at a variety of transverse distances. At both ends of the distance scale the radiation processes are, to a large extend, known. The small-size region is determined by QCD perturbation theory, the large-size domain by universal hadronic properties. This opens an attractive possibility of interpolation between these two extremes. First attempts in this direction have already been made, and, in particular, a simple model has been proposed which successfully describes the HERA data in the transition from perturbative QCD to nonperturbative strong interaction physics. HERA experiments have the potential further to increase the kinematically accessible measurement regions and to improve their measurement accuracy with increasing luminosity. This will considerably increase the amount of informations available for this challenging transition region.

The novel approach to the confinement problem has raised the question of understanding QCD radiation at large transverse distances. It is very tempting to recall another moment in the history of physics where the investigation of a "radiation" problem has led to unexpected and far-reaching results: the black body radiation in electromagnetism. In 1859 Kirchhoff had established that the energy distribution of black body radiation is universal, i.e. independent of the material of the black body. Shortly before the turn of the century Max Planck tried to find a theoretical derivation of a formula for the energy distribution J. In a first step he succeeded to interpolate between

two known limiting cases (the Raleigh-Jeans formula for small frequencies or long wave lengths, and Wien's law for high frequencies or short wave lengths). When trying to "derive" his interpolating formula he was forced to introduce the concept of "energy quantization", as the only way to explain the high frequency limit. This was the beginning of quantum theory, but it took another quarter of a century before the theory for the energy spectra of atoms was formulated, and then another few decades before Feynman and Schwinger presented the modern form of Quantum Electrodynamics which allows the calculation of scattering and radiation processes involving charged particles. It is this framework which nowadays also allows computation of the radiation of quarks and gluons in QCD at small distances. Now a new step in understanding radiation is needed: at large distances the QCD coupling becomes large, and confinement starts to radically change the radiation pattern. It seems natural to first define quantities which can be measured both at small and at large distances (analogous to the energy distribution J of the black body radiation). Presently the study of the quark-antiquark dipole cross section, $\sigma_{q\bar{q}p}$, is attracting much interest and future theoretical work will concentrate on deriving a theoretical formula for this quantity.

There is no doubt that HERA has opened a new door into the complicated dynamics of strong interaction forces. This article has attempted to provide a "Bestandsaufnahme". Understanding the dynamics of strong interactions remains one of the central tasks in particle physics. Also the search for fundamental theories beyond the Standard Model will find it necessary to have a better understanding of QCD dynamics: the development of new concepts (e.g. string theories) will need nonperturbative methods, for which QCD offers a challenging testing ground.

Acknowledgements. When writing this article we have profited from helpful discussions with many colleagues. Our special thanks go to A. Caldwell, B. Foster, K. Golec-Biernat, T. Haas, D.Haidt, R. Klanner, E. Levin, E. Lohrmann, A. Mueller, S. Schlenstedt, and G. Wolf.

References

1. V.N.Gribov, JETP 41 (1961) 667
2. A.Donnachie, P.V.Landshoff, Nucl.Phys. **B 244** (1984) 322
3. for a review see: A.B. Kaidalov, Physics Reports **50** (1979) 157; K. Goulianos, Physics Reports **101** (1983) 169
4. J.D.Bjorken, J.B.Kogut, D.E.Soper, Phys.Rev.**D 3** (1971) 1382
5. R.P.Feynman, Photon-Hadron Interactions, W.A.Benjamin, Inc.Publisher 1972
6. V.N.Gribov, in: Materials of the 8th Winter School of the Leningrad Institute of Nuclear Physics 1973 (in russian); hep-ph/0006158 (english translation)
7. H1 Collab., S. Aid et al., Nucl. Phys. **B 470** (1996) 4; ZEUS Collab. M. Derrick et al., Z. Phys. **C 72** (1996) 399; H1 Collab., C. Adloff et al., Nucl. Phys. **B 497** (1997) 3; ZEUS Collab. J. Breitweg et al., Phys. Lett. **B 407** (1997) 432; ZEUS Collab. J. Breitweg et al., Eur. Phys. J. **C7** (1999) 609; E665 Collab., M.R. Adams et al., Phys. Rev. **D 54** (1996) 3006; ZEUS Collab., J. Breitweg at al., DESY 00-071 (2000)
8. H1 Collab., S. Aid et al., Nucl.Phys. **B463** (1996) 3; ZEUS Collab., J. Breitweg et al., Eur.Phy.J. **C2** (1998) 247; ZEUS Collab., M. Derrick et al., Z.Phys. **C73** (1996) 1, 73; ZEUS Collab., M. Derrick et al., Phys.Lett. **B377** (1996) 259; H1 Collab., C. Adloff et al., Phys.Lett. **B483** (2000) 23; H1 Collab., C. Adloff et al., Eur.Phys.J. **C13** (2000) 371; ZEUS Collab., J. Breitweg et al., accepted by Phys.Lett. B-PLB 16283; H1 Collab., C. Adloff et al., Phys.Lett. **B483** (2000) 360; H1 Collab., C. Adloff et al., Eur.Phys.J. **C10** (1999) 373; for a review of data see: B. Mellado, http://arXiv.org/abs/hep-ex/0011050
9. ZEUS Collab. J. Breitweg et al., Eur. Phys. J. **C6** (1999) 43
10. A.D. Martin, R.G. Roberts, W.J. Stirling, Phys. Lett. **B387** (1996) 419
11. A.H. Mueller, 6th International Workshop on Deep Inelastic Scattering and QCD, DIS 98, (1998) 3, World Scientific
12. ZEUS Collab. J. Breitweg et al., Eur. Phys. J. **C1** (1998) 81;
13. K.Golec-Biernat, M.Wuesthoff, Phys.Rev. **D 59** (1999) 014017; Phys.Rev. **D 60** (1999) 114023
14. A. Levy, Phys. Lett. **B424** (1998) 191
15. S. Weinberg, Phys. Rev. **150** (1966) 1313; J. Bartels, M.G. Ryskin Z.Phys. **C76** (1997) 241
16. V.N.Gribov, L.N.Lipatov, Sov.J.Nucl.Phys **15** (1972) 78; G.Altarelli, G.Parisi, Nucl.Phys. **B126** (1977) 298; Yu.Dokshitzer, Sov.Phys.JETP **46** (1977) 641; for a review see: G.Altarelli, Phys.Rep. **81** (1982) 1
17. E.A.Kuraev, L.N.Lipatov, V. S. Fadin, Sov.Phys.JETP **45** (1977) 199; Ya.Ya.Balitskii, L.N. Lipatov, Sov.J.Nucl.Phys. **28** (1978) 822; for a review see: J.R.Forshaw, D.A.Ross, Quantum Chromodynamics and the Pomeron, Cambridge Lecture Notes in Physics 1997
18. A.H.Mueller "Small-x Physics, High Parton Densities and Parton Saturation in QCD", hep-ph/9911289